Advanced SYNCOM

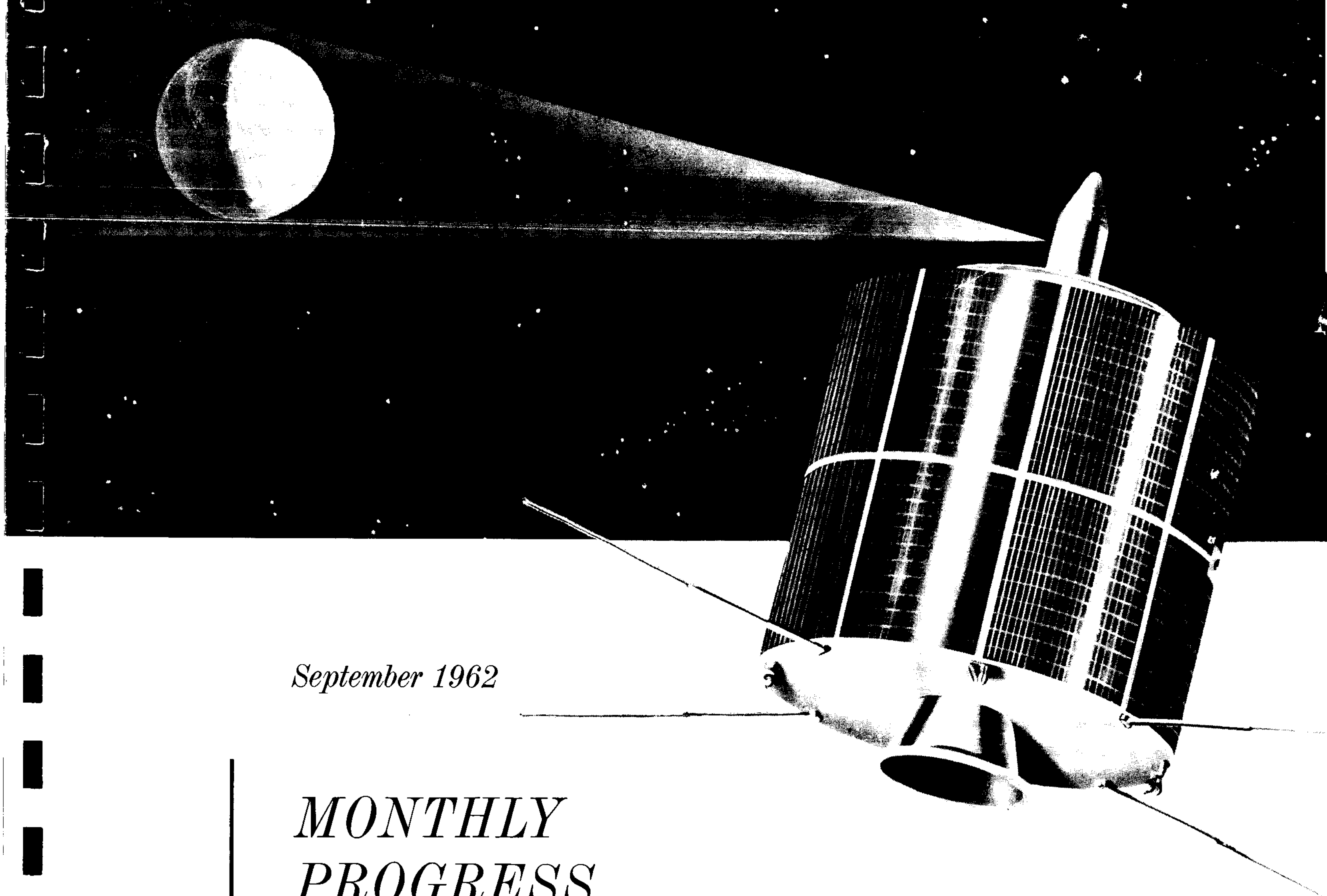

September 1962

MONTHLY PROGRESS REPORT

•

NASA Contract 5-2797
SSD 2473R

AEROSPACE GROUP
SPACE SYSTEMS DIVISION
HUGHES AIRCRAFT COMPANY
CULVER CITY, CALIFORNIA

HUGHES

Advanced SYNCOM

September 1962

MONTHLY PROGRESS REPORT

•

NASA Contract 5-2797
SSD 2473R

AEROSPACE GROUP
SPACE SYSTEMS DIVISION
HUGHES AIRCRAFT COMPANY
CULVER CITY, CALIFORNIA

HUGHES

HUGHES AIRCRAFT COMPANY

AEROSPACE GROUP

SPACE SYSTEMS DIVISION

CULVER CITY, CALIFORNIA

15 October 1962

SUBJECT: Advanced Syncom Monthly Progress Report for September 1962

TO: Mr. Alton E. Jones
Program Manager, Syncom
Goddard Space Flight Center
Code 621
Greenbelt, Maryland

Attached are copies of the Advanced Syncom Monthly Progress Report for September 1962.

The advanced technological development items progressed well through the report period. The developmental traveling-wave tube design was firmed and construction of the tubes initiated. Several of the transponder breadboard units have been completed, and design of the remaining units has been initiated.

A significant delay in completing the solid apogee motor specifications and hot gas control system specifications was encountered. Action has been taken to ensure completion of these documents during the month of October. The next reporting period should include finalizing of several additional transponder units and initiation of the procurement cycle of the hot gas control system.

HUGHES AIRCRAFT COMPANY

Harold A. Rosen for
C. Gordon Murphy
Program Manager
Project Syncom

cc: H. E. Tetirick
Goddard Space Flight Center
Code 241
Greenbelt, Maryland

TABLE OF CONTENTS

1. INTRODUCTION

Under NASA Goddard Space Flight Center Contract NAS-5-2797, Hughes Aircraft Company is conducting feasibility studies and advanced technological development for an advanced, stationary, active repeater, communication satellite.

An Initial Project Development Plan, submitted to Goddard on 15 August 1962, reported the initial system feasibility studies and delineated technical approaches, the administrative plan, manpower requirements, schedule, and funding considerations appropriate for accomplishing the NASA contract objectives.

These monthly technical letter reports present the technical progress made during the reporting period, the critical problems or delays encountered, and the plans for the forthcoming reporting period.

Separate reports of schedule status are provided through biweekly PERT reports. Monthly Financial Management reports provide the funding status.

2. SYSTEM DESIGN STUDY

ORBIT/TRAJECTORY ANALYSES

An IBM 7090 computer program for the computation of boost-coast trajectories (allowing up to six primary propulsion stages) has been completed, checked, and documented. This three-dimensional program includes earth's oblateness, allows for winds and rail launch, and provides station observables and conic parameters. It also incorporates a subroutine that permits searching for those stage parameter values yielding a trajectory with prescribed terminal conditions. This program will provide accurate evaluation of existing booster performance in addition to serving as a tool for preliminary design.

Because the program allows for any combination of boost and coast periods, payload optimization for different parking orbit altitudes of the Atlas-Agena vehicle may be studied to determine the "best" parking orbit altitude for a given final longitude placement. The best parking orbit altitude may be that altitude which yields the maximum injected payload with negligible drag effects when in the parking orbit and during the perigee passage when in the transfer orbit (should such an ascent sequence be indicated).

SPACECRAFT/ORBIT DYNAMICS

Gross Effects of Ground Control Loss on Advanced Syncom

In this section are the results of several perturbation studies to predict the gross behavior of an initially stationary orbit after loss of ground control commands that normally remove the effects of the two perturbation sources, the triaxiality of the earth and the sun-moon gravitational attraction. In addition, an examination is made of the effect of using mean instead of apparent sun position as a despinning reference for positioning the antenna pencil beam over the earth after loss of ground control. Finally, the estimated maximum magnitudes of attitude disturbing torques due to the effects of gravity gradient, magnetic field, and solar radiation pressure unbalance are reported.

Triaxiality of the Earth

The effects of the nonspherical mass distribution of the earth on a nominally stationary satellite have been examined at Hughes (Reference 1), Rand Corporation (Reference 2), and NASA (Reference 3), among others. Of particular importance is the effect of the ellipticity of the earth's equatorial section. If the earth's gravitational potential in the equatorial plane at the synchronous radius r_c is given by

$$U_{eq} = \frac{g_o R_e^2}{r_c} \left[1 - J_2 \frac{R_e^2}{2r_c^2} + 3 J_2^{(2)} \frac{R_c^2}{r_c^2} \cos 2 (\lambda - \lambda_o) \right]$$

where

R_e = earth's radius ≅ 3441.7 nautical miles

r_c = synchronous radius ≅ 22,752.5 nautical miles

g_o = gravitational acceleration at the earth's surface

$g_o R_e^2 = k^2$ = earth's constant of attraction
= 62,627.75 n. mi.^{3}/sec^2

J_2 = coefficient of zonal harmonic (earth oblateness)
= + 1.08219 x 10^{-3}

$J_2^{(2)}$ = coefficient of tesseral harmonic (Reference 3) (equatorial ellipticity)
= - 2.2 x 10^{-6}

λ = instantaneous satellite longitude (positive eastward)

λ_o = longitude of minor axis of equatorial ellipse

The Rand study shows that the time t to drift through a longitude change $|\Delta\lambda| \leq 10$ degrees is given approximately by

$$\Delta\lambda \cong 9 J_2^{(2)} \frac{R_e^2}{r_c^2} \omega_e^2 t^2 \sin 2 (\lambda_i - \lambda_o)$$

where

ω_e = earth's rate = 2π radians per day

λ_i = initial longitude of satellite at time of control loss, $t = 0$

Since the exact location of λ_o is yet to be determined, the worst case drift rate (e.g., $|\lambda_i - \lambda_o| = 45$ degrees) will be considered, using the latest reported value of $J_2^{(2)}$ (Reference 3). Thus,

$$|\Delta\lambda|_{max} = (9)(2.2 \times 10^{-6})(0.15127)^2 (6.28)^2 (57.3)\left[\frac{\text{deg}}{\text{day}^2}\right] t^2$$

$$= 1.025 \times 10^{-3} \left[\frac{\text{deg}}{\text{day}^2}\right] t^2$$

Figure 2-1 is a log-log plot of the above expression showing that the satellite will drift 0.05 and 0.1 degree after 7 and 10 days, respectively, due to the ellipticity of the earth's equatorial section. The drift is toward the minor axis λ_o or $\lambda_o + \pi$, whichever is closer, since these locations represent positions of stable equilibrium. In general, the satellite will execute large-angle oscillations in the equatorial plane about the minor axis. The period of oscillation will depend on the initial longitude of the satellite relative to the longitude of the minor axis, i.e. $|\lambda_i - \lambda_o|$. For $|\lambda_i - \lambda_o| = 45$ degrees, the period T is about 2.4 years. This period reduces to a little over 2 years as $|\lambda_i - \lambda_o|$ approaches zero and increases rapidly to over 5 years as $|\lambda_i - \lambda_o|$ approaches 90 degrees. The semiamplitude of these oscillations is equal to the initial longitude difference between the satellite and the nearest minor axis, $|\lambda_i - \lambda_o| \leq 90$ degrees.

It is interesting to note that as $|\lambda - \lambda_o|$ is increasing, the orbital radius r_c decreases by an amount δ_r; conversely, when $|\lambda - \lambda_o|$ is decreasing, δ_r is positive. The maximum change in δ_r occurs when the satellite passes the location of the minor axis and is given by

$$\left|\frac{\delta_r \max}{r_c}\right| = 4\sqrt{-J_2^{(2)}}\ \frac{R_e}{r_c} \sin\left|\lambda_i - \lambda_o\right|$$

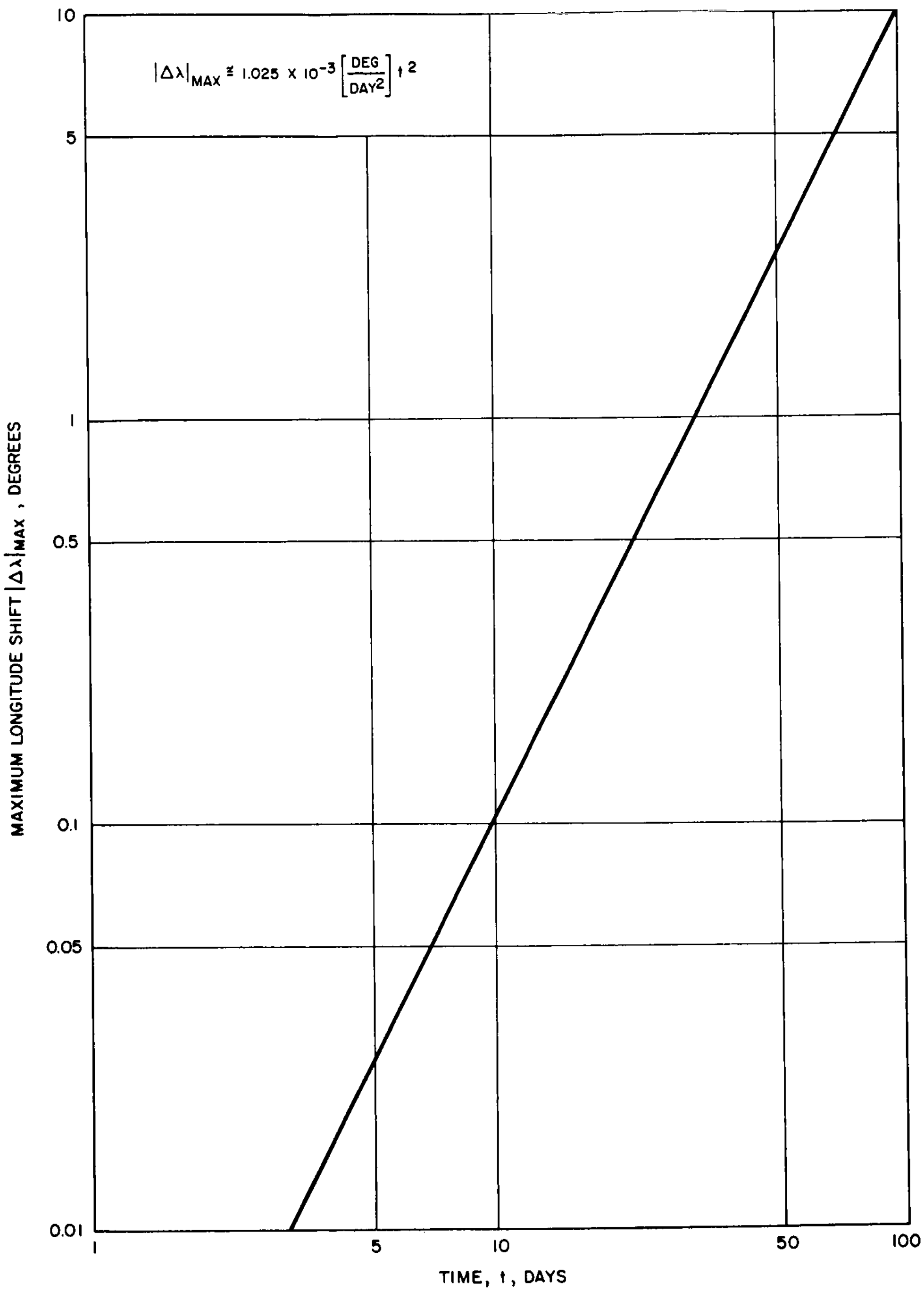

Figure 2-1. Maximum Longitude Shift of Stationary Satellite due to Earth Triaxiality Perturbation

or

$$\left|\delta_{r_{max}}\right| \cong 20.4 \sin \left|\lambda_i - \lambda_o\right| \text{ nautical miles}$$

$$0 \leq \left|\lambda_i - \lambda_o\right| \leq 90 \text{ degrees}$$

Finally, the triaxiality of the earth causes no change in the inclination of an equatorial synchronous orbit, and the maximum control system velocity increment required to correct to in-plane effect is about 7 fps per year as reported in Reference 3. In the Project Development Plan, 15 August 1962, the value used for $J_2^{(2)}$ was about (-5.5×10^{-6}), yielding 17.7 fps for the required velocity correction.

Sun-Moon Effects

The main effect of the sun and the moon is to cause the inclination of the stationary orbit to increase at the maximum rate of about 0.95 degree per year (0.8525 degree per year, according to Reference 2) for the first 10 to 15 years after ground control loss. This results in a north-south oscillation of the satellite with a period of 1 sidereal day and with an amplitude that increases with the above rate. Of this amplitude rate, the moon contributes a maximum of about 0.685 degree per year, and the sun contributes 0.27 degree per year.

An approximate expression for the inclination increase, Δi_p, with time, t, for a perturbing body p is given by

$$\Delta i_p \cong A_p \left[(n_p t)^2 + \sin^2 (n_p t) - 2\, n_p t \cos (n_p t + 2\, v_{po}) \right]^{1/2}$$

where

$$A_p = \frac{3}{4} \frac{k_p^2}{n_o R_p^3 n_p} \sin I_p \cos I_p$$

k_p^2 = constant of attraction of perturbing body

n_o = stationary satellite angular velocity = ω_e = 2π radians per day

n_p = perturbing body angular velocity

R_p = distance between centers of earth and perturbing body

I_p = inclination angle of perturbing body orbit plane to earth equatorial plane

v_{po} = initial polar angle of perturbing body relative to satellite at $t = 0$

Now, for the moon, we have

$$k_p^2 = k_m^2 = 0.0123\ k^2$$

$$n_p \cong \frac{2\pi}{27.3} \text{ radians per day} = n_m$$

$$I_p = I_m \text{ where } 18.317 \text{ degrees} \leq I_m \leq 28.584 \text{ degrees}$$

$$R_p = R_m \cong 60.267\ R_e$$

$$A_p = A_m \leq 0.00814 \text{ degree}$$

For the sun, we write

$$k_p^2 = k_s^2 = 333,000\ k^2$$

$$n_p = n_s \cong \frac{2\pi}{365.25}\ \frac{\text{rad}}{\text{day}}$$

$$I_p = I_s = 23.45 \text{ degrees}$$

$$R_p = R_s \cong 2.34 \times 10^4\ R_e$$

$$A_p = A_s \cong 0.0432 \text{ degree}$$

Figure 2-2 is a plot of the inclination increase due to the sun and moon as a function of the polar angle of the perturbing body where $v_{po} = 0$. The effect of the diurnal motion has been averaged out over one orbital period (24 hours). The figure shows that the moon will induce an inclination increase of about 0.05 degree at the end of 1 sidereal month (27.3 days), while the sun will cause this inclination change at the end of 68.5 days. It will take approximately twice as long to accrue an inclination of 0.1 degree due to the sun and moon.

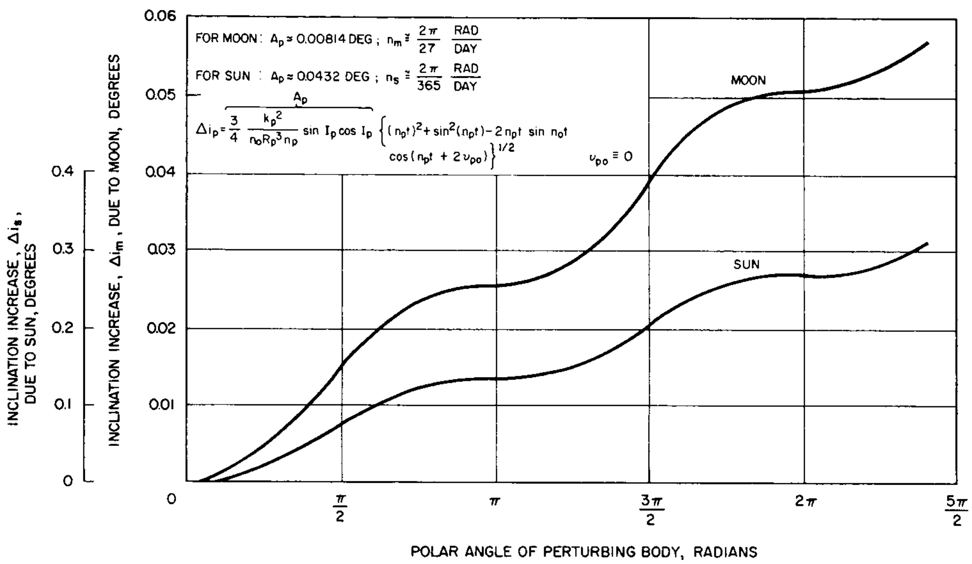

Figure 2-2. Stationary Satellite Inclination Change due to Sun-Moon Perturbations

It should be noted, however, that even if the inclination magnitude exceeds the ground antenna pointing angle limits with respect to satellite latitude deviations, the diurnal oscillation will cause the satellite to cross the equator twice a day and come within the pointing angle limits of the ground antennas for at least a fraction of each day (assuming no longitudinal drift due to triaxiality). Thus, if the satellite initial longitude is located close enough to a minor axis of the equatorial ellipse so that the resultant longitudinal drift rate is made comparable to the rate of increase of inclination due to the sun and moon, the useful continuous communication period (after ground control loss) of the satellite can be optimized with respect to the ground antenna pointing limitations. A similar argument holds for providing communication periods equal to some minimum fraction of a day (resulting in a required satellite longitudinal placement closer to the minor axis than for the continuous communication case).

Finally, the in-plane effect of the sun-moon perturbation on the satellite orbit is shown to be small from a ground antenna tracking standpoint (Reference 2). In particular, the maximum possible tangential deviation from an initial longitudinal position is less than 39 nautical miles, or about 7 minutes of arc as seen from the earth's surface.

Effect of Equation of Time on Syncom Pencil-Beam Pointing

The relative longitude of the sun with respect to the satellite is shown to be (Reference 4)

$$\lambda_s = \lambda_i - 180 \text{ degrees} - \omega_e (UT + E) \quad \text{(degrees)}$$

where

λ_i = initial longitude of satellite in degrees east of Greenwich

ω_e = earth's rate of rotation = 15 degrees per hour

UT = Greenwich mean time (Universal Time), hours

E = equation of time

= apparent (true) minus mean right ascension of sun, hours

Thus, λ_s is the angle between the projection of the satellite-sun line onto the equatorial plane and the upward local vertical of the satellite location. This is used as the despinning reference angle for pointing the maximum gain of satellite pencil-beam pattern along the local vertical toward the earth. When the ground control link is operative, the correct value of E can be periodically commanded to make up for the seasonal changes in the difference between the mean sun and apparent sun position. If, at $t = o$, ground control is lost, the subsequent pointing error $\delta\lambda$ of the pencil-beam maximum is given by

$$\delta\lambda = \omega_e \int_o^t \frac{\delta E}{\delta t} \, dt$$

where

$\delta E/\delta t$ = daily rate of change of E tabulated in the American Ephemeris and Nautical Almanac

ω_e = earth's rate

= 15 degrees per hour

Although $\delta E/\delta t$ is essentially a periodic function for each year of the form (where $|a_o|, |a_3|, |a_4| < |a_1| < |a_2|$)

$$\frac{\delta E}{\delta t} = a_o + a_1 \cos 2\pi \frac{(t - t_o)}{365} + a_2 \cos \frac{4\pi (t - t_o)}{365}$$

$$+ a_3 \cos \frac{6\pi (t - t_o)}{365} + a_4 \cos \frac{8\pi (t - t_o)}{365}$$

it cannot be directly integrated until the reference date $t = 0$ is known relative to the beginning of the year t_o. However, some upper bounds can be established.

An examination of the American Ephemeris for 1962 and 1963 shows that the position of the hour angle of the mean sun is never more than 16 minutes (of time) or 4 degrees from the true sun, with a peak-to-peak variation δE_{max} of 29.5 minutes (1770 seconds) or 7.4 degrees. Furthermore, the maximum value of the rate of change of E is

$$\left(\frac{\delta E}{\delta t}\right)_{max} = 30 \frac{\text{seconds}}{\text{day}}$$

Thus, under the worst conditions, such as ground control loss when $\delta E/\delta t$ is maximum,

$$\delta\lambda_{max} = \omega_e \left\{ \min\left[\left(\frac{\delta E}{\delta t}\right)_{max} t, \ \delta E_{max} \right] \right\}$$

$$= 0.004167 \left\{ \min\left[30\ t,\ 1770 \right] \right\} \quad \text{(degrees)}$$

$$= \text{minimum}\left[0.125\ t,\ 7.4 \right] \quad \text{(degrees)}$$

where t is in days. Now for a $\frac{\sin k\,\theta}{k\,\theta}$ pencil-beam pattern whose gain is 3 db down at $\theta = 8.6$ degrees, the 2-db down point occurs at $\theta = 7$ degrees from the local vertical. If this angle constitutes the allowable pointing error $\delta\lambda_a$ for usable communication signal strength, it will take at least 56 days after ground control loss to accrue 7 degrees. If a pointing error of 7.4 degrees still provides useful signal strength for certain land masses (east or west of the satellite nadir, depending upon the direction of the shift of the pencil beam which, in turn, depends on the year and season of ground control loss), the maximum useful time interval for operation after ground control loss will be determined only by ground antenna tracking limitations in the face of perturbation-induced drifts, as discussed earlier.

Disturbing Torques (References 4 and 5)

Gravity Gradient. Since the spin axis is normal to the plane of the orbit, the dominant inverse squared term of gravitational attraction does not give rise to any torque on the satellite. Furthermore, since the initial orbit is in the equatorial plane, the torque, due to oblateness, will be initially zero. To estimate the order of magnitude of gravity gradient precession rate due to the sun-moon induced inclination increase of the satellite orbit, Williams (Reference 5) observes that in the inverse square field this rate is given by

$$\left| \dot{\psi}_g \right| \cong 3\, g_o \frac{R_e^{\,2}}{r_c^{\,3}} \frac{(I_z - I_x)}{I_z\, \omega_z} \left(\frac{\delta i}{\delta t}\right) t = 3.6 \times 10^{-10} \left[\frac{\text{deg}}{\text{sec-yr}} \right] t$$

where

R_e = earth's radius

g_o = surface gravity at R_e

r_e = stationary orbital radius

I_z = moment of inertia about the spin axis

= 50.6 slug-ft^2 (half-life value) (Reference 6)

I_x = moment of inertia about normal to spin axis

= 37.8 slug-ft^2 (half-life value) (Reference 6)

ω_z = satellite spin rate

= 100 rpm = 10.5 rad/sec

$\left(\frac{\delta i}{\delta t}\right)$ = sun-moon induced inclination rate of stationary orbit

$\leq$ 0.95 deg/yr = 1.66 x 10^{-4} rad/yr

The maximum precession rate due to oblateness is shown to have the order of magnitude of

$$\left|\dot{\psi}_{g_o}\right|_{max} = \frac{3\, g_o\, R_e^4}{2\, \omega_z\, r_c^5} J_2 = 19.2 \times 10^{-6} \frac{\text{deg}}{\text{yr}}$$

<u>Magnetic Field</u>. Two effects result from eddy currents in the satellite induced by the presence of a magnetic field:

1) The spin speed ω_z is damped, $d\,\omega_z/dt < 0$.

2) The spin axis precesses toward the instantaneous magnetic field.

For an electrically symmetrical structure, Williams (References 4, 5, and 7) shows that the precession rate $\dot{\theta}$ and spin speed $\dot{\omega}_z$ can be conservatively represented by

$$\theta = -\frac{\sin\theta\cos\theta}{\tau_o}$$

$$\dot{\omega}_z = -\frac{\sin^2\theta}{\tau_o}\,\omega_z$$

$$\tau_o = \frac{2\rho}{\sigma B_o^2} = \text{minimum damping constant}$$

where

θ = angle between the spin axis and the magnetic field

ρ = density of idealized satellite cylindrical shell (with massles perfectly conducting end planes)

= 2650 kg/m^3 for aluminum

σ = specific surface conductivity

= 3.54 mhos/meter for aluminum

B_o = magnetic field induction at r_c due to earth's magnetism

$\leq 0.630 \left(\frac{R_e}{r_c}\right)^3$ gauss

$\leq 2.18 \times 10^{-7}$ Webers/meter^2

Thus,

$$\tau_o = \frac{1.5 \times 10^{-14}}{4.74 \times 10^{-14}} = 3.165 \times 10^9 \text{ seconds} = 100 \text{ years}$$

$$\dot{\theta} = - \frac{0.56}{2 \times 100} = - 2.8 \times 10^{-3} \text{ radians per year} = - 0.16 \text{ degrees per year}$$

$$\dot{\omega}_z / \omega_z = - \frac{0.0852}{100} = - 0.852 \times 10^{-3} \text{ radians per year}$$

Hysteresis effects may contribute additionally to the damping of spin, but predictions at this time may be premature. However, a conservative estimate may be made by comparing with some spin speed decay data of Telstar due to hysteresis (Reference 8). If the spin speed ω_z obeys an exponential decay law

$$\omega_z = \omega_{zo} e^{-t/\tau_h}$$

then the Telstar data exhibits a time constant, τ_h, of

τ_h = 320 days

Now, since the perigee and apogee altitudes of Telstar are about 515 and 3043 nautical miles respectively, the field strength is about 300 times that of a synchronous satellite, so that the hysteresis decay time constant should be considerably longer for Syncom.

The precession rate due to the torque created by the magnetic moment of the satellite and the earth's magnetic field B_o is also expected to be small at the synchronous radius. If the magnetic moment is expressed in (ampere-turns-meters^2), the precession rate $\dot{\theta}_m$ may be estimated by (Reference 7)

$$\dot{\theta}_m \approx \frac{B_o niA \sin\theta}{I_z\ \omega_z} \; ; \quad \frac{\dot{\theta}_m}{niA \sin\theta} \approx 3 \times 10^{-10} \frac{\text{rad/sec}}{\text{amp-turn-m}^2}$$

$$= \frac{0.053 \text{ deg/yr}}{\text{amp-turn-m}^2}$$

where

ni = magnetic-moment-inducing current (ampere turns)

A = area enclosed by current loop (meters^2)

θ = angle between B_o and normal to A

B_o = earth's field strength at r_c

$= 2.18 \times 10^{-7}$ Weber/meter^2

$I_z \cong 50.6$ slug feet^2 $= 50.6 \times 1.36 = 69$ kg - m^2 = 69 Newton-meter-second^2

ω_z = 10.5 rad/sec

<u>Solar Radiation</u>. Solar radiation pressure unbalance is the most significant torque yet estimated. A simple model for calculating this effect is a cylinder with perfectly reflecting ends and completely absorbing sides. Consideration of the varying geometry during the course of a year shows that there is an average precession of the spin axis in the direction of the intersection of the orbital (equatorial) plane (normal to the initial spin axis) and the ecliptic plane. By integrating the precession rate, Williams (Reference 4) shows that the magnitude is

$$\bar{\dot{\psi}} = \frac{\pi}{8} \frac{S}{C} a^2 h \frac{\sin 2i}{I_z\ \omega_z}$$

where

S/C = ratio of solar constant to speed of light

$= 0.957 \times 10^{-7}\ \text{lb/ft}^2$

$= 0.957 \times 10^{-7}\ \text{slug/ft - sec}^2$

a = radius of the cylinder

= 23.5 inches = 1.96 feet

h = height of the cylinder

= 25 inches = 2.08 feet

i = inclination of the orbit to the ecliptic

= 23.6 degrees

$I_z = 50.6\ \text{slug-ft}^2$

$\omega_z = 10.5\ \text{rad/sec}$

Thus, the maximum precession rate magnitude is

$$\bar{\dot{\psi}} = 4.13 \times 10^{-10}\ \frac{\text{rad}}{\text{sec}} = 0.013\ \frac{\text{rad}}{\text{yr}} = 0.75\ \frac{\text{deg}}{\text{yr}}$$

INTERFACE WITH AGENA-D

The coordination conducted with Goddard and the Lockheed Missiles and Space Company (LMSC) has been addressed primarily to three areas: the structural dynamic interactions among the Syncom II spacecraft, the interconnect and bearing table structure, and the Agena-D vehicle; the mechanical, environmental, and electrical interfaces; and the exchange of synchronous orbit injection performance parameters and requirements.

The utility of the dynamic environmental developmental tests to be performed on the engineering model structure would be greatly enhanced by the use of an actual interconnect structure, bearing table, and mechanical interface. Vibration and acceleration inputs would thus be made at the Agena-D, and proper frequencies and magnification factors could then be determined. Overall program savings could potentially accrue from this approach, because the special test fixture that simulates this equipment would then not be required and because a more realistic representation of the launch environment could be obtained.

Design of the interstage must include adequate provisions for RF checkout of the communication systems on the launch pad and should give consideration to the possible operation of the communication system throughout launch and orbit injection.

Preliminary Mark II launch pad air conditioning requirements are as follows:

Payload heat dissipation:

100 watts of 2.5-watt traveling-wave tubes

125 watts of 3.0-watt traveling-wave tubes

200 watts of 5.0-watt traveling-wave tubes

Temperature limits of ambient air under shroud cover:

+50°F to +80°F.

Relative humidity:

20 to 50 percent

Dust particle size and count:

Particle Size, microns	Count, per cubic feet	Total Count per cubic foot
1.0 to 15.0	140,000	
15.1 to 30.0	96,500	
30.1 to 55.0	13,500	Not over 250,000
55.1 to 70.0	2,500	
Over 70.0	1,000	

The assembly test and transport areas should provide equivalent environments.

Based upon information provided by Goddard and LMSC, preliminary unit response estimates have been derived; the tabulated estimates are at qualification levels. Responses act through the component center of gravity in the indicated direction. Lateral responses act in any radial direction. The total response of components not listed is estimated to be 50 g.

Environments

Sinusoidal Excitation (all three axes, log sweep at 2 octaves per minute, 4.6 minutes duration):

5-15 cps	0.25-inch double amplitude
15-250 cps	3 g peak
250-400 cps	5 g peak
400-3000 cps	7.5 g peak

Random Excitation (6 minutes along each of three axes):

20-80 cps	0.04 g^2/cps
80-1280 cps	Increasing from 0.04 g^2/cps at 1.22 db/octave
1280-5000 cps	0.07 g^2/cps

Shock Excitation (applied only to components, three shocks in each direction):

Longitudinal: 30 g sawtooth pulse of 0.015 second duration.
Lateral: 15 g sawtooth pulse of 0.015 second duration.

Responses

	Maximum Longitudinal Response, g 0-Peak, approximately 80 cps	Maximum Lateral Response, g 0-Peak, approximately 40 cps
Antenna electronics	30	30
Traveling-wave tubes	30	30
Electronics packages	30	30
MMH and N_2 tanks	30	30
Telemetry transmitter	18	30
Converter	18	30
Solar panel	30	30
Battery pack	30	30
Thermal switch	18	30
Nutation damper	30	30

The general transmissibility envelope for components is given in Table 2-1.

TABLE 2-1. COMPONENT TRANSMISSIBILITY ENVELOPE

Frequency, cps	Longitudinal Amplification	Lateral Amplification
5-20	5	5
20-60	5	10
60-100	10	5
100-300	5	5
300-500	2	2
500-2000	1	1

SYSTEM RELIABILITY STUDIES

System reliability studies during the reporting period included 1) an analysis of the probability of mission success for each communications mode, 2) modification of the reliability program for the IBM 7090 computer to incorporate the launch sequence effects on orbital reliability, 3) a preliminary examination of the command subsystem to determine weight-redundancy (reliability) tradeoffs, and 4) a general updating of the reliability diagram to include the design and modification of units and subassemblies.

The reliability section of the Initial Project Development Plan (IPDP) presented lifetime curves for total communications, i.e. the multiple access mode and frequency translation mode combined, and telemetry for the orbital mission phase. This analysis was based upon the assumption that both receivers operate simultaneously at 100-percent duty cycle (a conservative estimate) and that the survival of one frequency translation receiver would be adequate for successful communication. Since each receiver or mode may not operate simultaneously, an analysis has been performed to determine the reliability of each communications mode during the orbital mission, again assuming a 100-percent duty cycle (worst case analysis) for each. The results yield lifetime curves expressing the probability of successful multiple access (Figure 2-3) and frequency translation (Figure 2-4) communications for at least one, two, three or four effective quadrants surviving a discreet mission period. These lifetime curves superimposed form envelopes for each quadrant plot which determine minimum and maximum reliability limits for the spacecraft communication system operating 100-percent of the time. This may be more readily visualized by a plot of 50-percent probability of survival intercepts for each mode, Figure 2-5. Further definition and allocation of each transponder mode duty factor will again provide composite lifetime curves for total communications which should fall between the limits presented. However, these estimates are based upon the IPDP spacecraft configuration and preliminary unit reliability estimates, which will necessarily be updated as the spacecraft configuration is detailed and confirmed.

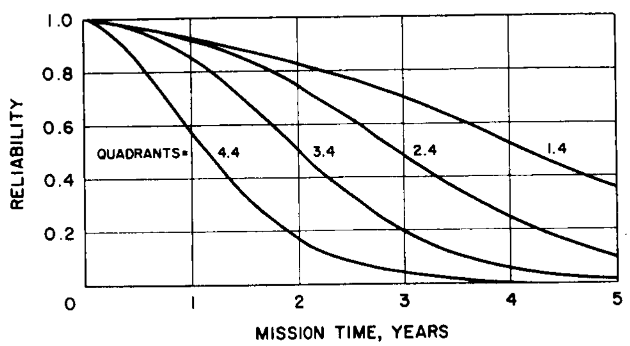

Figure 2-3. Probability of Successful Communications Single-Sideband Mode

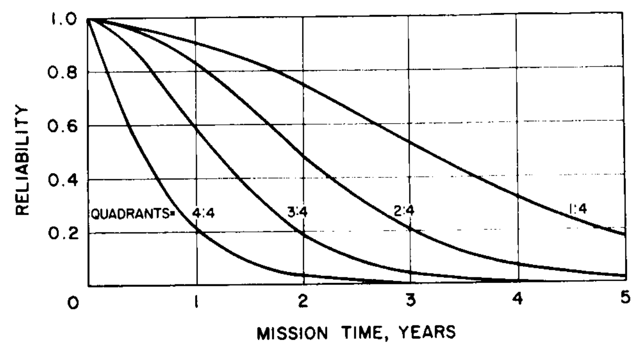

Figure 2-4. Probability of Successful Communications - Frequency Translation Mode

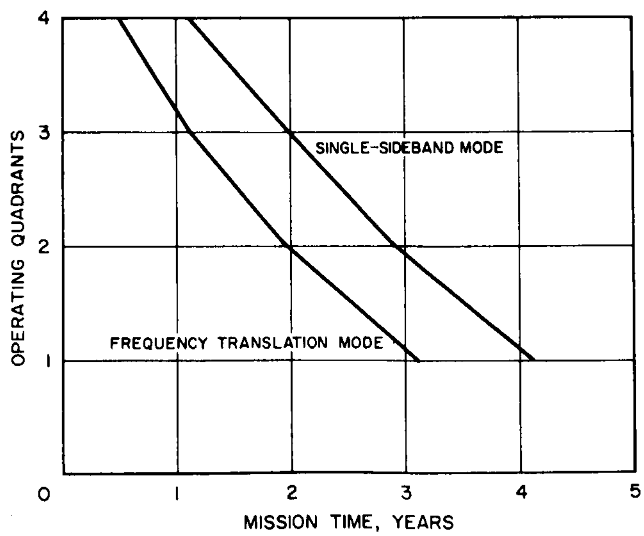

Figure 2-5. 50 Percent Probability of Quadrant Survival

The mathematical model representing the orbital configuration during either communications mode may be expressed by the following equations for reliability, with the characters defined by the IPDP.

Multiple Access Communication Mode

$$R_{SSC} = (R_B R_{SO}) \Bigg[\sum_{r=1,2,3,4}^{4} \frac{4!}{(4-r)!\,r!} \left[R_{CX}(1 + P_s\lambda_{cx}t) R_{MA}(1 + P_s\lambda_{ma}t)\right]^r$$

$$\left[1 - R_{CX}(1 + P_s\lambda_{cx}t) R_{MA}(1 + P_s\lambda_{ma}t)\right]^{4-r} \Bigg]$$

$$\left[1 + P_s\lambda_c t + \frac{P_s^2(\lambda_c t)^2}{2!} + \frac{P_s^3(\lambda_c t)^3}{3!}\right] R_{DB}\left[1 - (1 - R_{DA} R_{RC})^2\right]$$

$$R_{AC} R_{SS}\left[1 + P_s\lambda_a t + \frac{P_s^2(\lambda_a t)^2}{2!} + \frac{P_s^3(\lambda_a t)^3}{3!}\right]$$

$$R_{CXA} R_{CRA} R_{TA}\left[1 - (1 - R_{VOC} R_J)^2\right] R_{PS}$$

Frequency Translation Communication Mode

$$R_{FTC} = (R_B R_{SO}) \Bigg[\sum_{r=1,2,3,4}^{4} \frac{4!}{(4-r)!\,r!} \left[R_{CX}(1 + P_s\lambda_{cx}t) R_{FT}\right]^r$$

$$\left[1 - R_{CX}(1 + P_s\lambda_{cx}t) R_{FT}\right]^{4-r} \Bigg] \left[1 + P_s\lambda_c t + \frac{P_s^2(\lambda_c t)^2}{2!} + \frac{P_s^3(\lambda_c t)^3}{3!}\right]$$

$$R_{DB}\left[1 - (1 - R_{DA} R_{RC})^2\right] R_{AC} R_{SS}\left[1 + P_s\lambda_a t + \frac{P_s^2(\lambda_a t)^2}{2!} + \frac{P_s^3(\lambda_a t)^3}{3!}\right]$$

$$R_{CXA} R_{CRA} R_{TA}\left[1 - (1 - R_{VOC} R_J)^2\right] R_{PS}$$

An essential reliability study in this program is the determination of mission reliability incorporating the launch sequence reliability, boost and synchronization-orientation. The mathematical analysis of the probability of survival through the launch sequence and its effect upon the orbital phase reliability is more subtle and complex than might be expected. In the case of a nonredundant system, the overall mission reliability may be simply expressed by the product of the equipment survival probabilities for each mission phase sequence. However, in a highly redundant system such as the Advanced Syncom spacecraft, this technique provides an incomplete mathematical model. It might be suggested that the probability of survival of redundant equipment through a particular phase sequence, such as boost, be computed independently of the following phases and the result multiplied by the reliability of the following sequence, such as orbit, which is computed from accepted expressions of redundancy. Here it must be recalled that the preliminary orbital analyses in the IPDP were based upon the assumption that all equipment survived the launch sequence; in other words, the launch sequence reliability was assumed equal to one. By the technique described in the IPDP, the probability of one equipment failing and the second remaining operable, considering a redundant pair, was not included in the mathematical analysis. Therefore, a more correct method is to define the equations that describe all possible modes of survival for redundant equipment that undergoes multiple mission phase sequences in its lifetime, such as launch and orbit in the Syncom application. For parallel operation of equipment, the general equation may be written as

$$R_p = 1 - (1 - \prod_{i=1}^{n} R_i)^m$$

where

R_p = the reliability of the parallel combination

n = number of mission phase sequences

R_i = reliability of the equipment during the i^{th} phase sequence

m = number of redundant equipment

The general expression for reliability of equipment in a standby configuration may be written as

$$R_s = \sum_{q=1}^{s} \left[\frac{s!}{(s-q)!\,q!} \prod_{i=1}^{n-1} R_i^q R_n \left(1 - \prod_{i=1}^{n-1} R_i\right)^{s-q} \left[P_s \lambda t + \frac{P_s^2 (\lambda t)^2}{2!} + \dots \frac{P_s^{q-1} (\lambda t)^{q-1}}{(q-1)!} \right] \right] + \sum_{r}^{s} \frac{s!}{(s-r)!\,r!} \prod_{i=1}^{n-1} R_i^r R_n \left(1 - \prod_{i=1}^{n-1} R_i\right)^{s-r}$$

where

R_s = reliability of the standby configuration

s = number of equipment in the standby configuration

q = an integer $0 < q \leq S$

n = number of mission phase sequences, i. e. boost, synchronization-orientation, orbit (3)

R_i = reliability of one equipment during the i^{th} phase sequence

R_n = reliability of one equipment during the final phase sequence

P_s = probability of successful operation of the switching function

λ = failure rate of one equipment during the n^{th} phase sequence

t = specified time associated with the n^{th} sequence

r = an integer $= q + 1 \qquad 1 < c \leq s$

As noted above, the general expression for a series equipment is simply

$$R = \prod_{i=1}^{n} R_i$$

where

R = reliability of the series equipment

n = number of sequence intervals

R_i = reliability of the equipment during the i^{th} sequence interval

These equations have been developed by an examination of survival probabilities for each sequence interval and the effect of equipment failure or survival upon subsequent intervals. Although the development of these expressions may not be readily apparent, the formulation of a "truth table" will validate their applicability to a reliability analysis of multiple mission phase sequences.

The computer program developed for the reliability analysis of the Advanced Syncom spacecraft configuration has been updated during this report period to include these equations and the general capability to evaluate multiple sequence reliability. It is expected that the following progress reports will include the redefinition of the spacecraft mathematical model incorporating boost, synchronization-orientation, and orbital reliabilities in the terms described, along with lifetime curves. It may be noted that the mathematical model described in the IPDP is essentially accurate and includes the boost (R_B) and synchronization-orientation reliabilities (R_{SO}). However, the derivation of $R_B R_{SO}$ is not straightforward and, therefore, the technique described herein has been developed to include the effects of these sequence intervals upon the orbital reliability.

The mathematical model has been developed in sufficient detail to proceed with related studies of launch and orbital operations in order to determine the limits to be expected of such parameters as launch rate to establish the initial system availability as a function of continued launch rate, system replacement criteria, and other operations analyses.

A preliminary examination of the command subsystem to determine tradeoffs has also been undertaken. It is readily apparent that these tradeoffs will be determined by the number of channels required by the decoders, something yet to be defined. Therefore, the present recommendations will depend, too, upon the number of decoder channels required. This analysis has shown that, for the present spacecraft configuration (55 decoder channels), a substantial gain in reliability is experienced by having at least three quadrants of command. The reliability gain for the fourth quadrant of command is small but may become significant as the complexity of the decoder increases. Results of the analysis will be published in a later report.

In addition to the tasks described above, a general upgrading of the reliability diagram and its component parts is in process. This upgrading is a continual process required as the design is defined and tradeoffs during the developmental program occur. Revised unit and subsystem reliability objectives and estimates based upon accurate component information and further analyses and definition of the Syncom mission will be formulated as the design matures and will be given in later reports.

COMPONENTS AND MATERIALS

A cross-reference list of vendor part numbers for resistors, capacitors, and semiconductors in the Preferred Parts List is being prepared to aid circuit designers in the initial use of preferred parts. This list should be completed during the next report period.

Mark I drawings are being re-examined to determine if components used in Syncom I should be modified for Syncom II.

Elements of the ferrite phase shifter for the transmitting antenna system have been examined; both the ferrite and insulating material are acceptable for space environment. The material in which the electromagnetic coil is dipped is now being examined in vacuum. If it is satisfactory, fully acceptable coils may be ordered, with one additional change of material to be incorporated by the vendor.

REFERENCES

1. Williams, D. D., "Triaxiality of the Earth and its Effect on a Stationary Satellite," Hughes Aircraft Company TIC 4120. 7/13, 30 December 1960.

2. Frick, R. H. and T. B. Garber, "Perturbation of a Synchronous Satellite," Rand Corporation, R-399 NASA, Contract NASr-21 (02), May 1962.

3. Fleig, A. J., "Effect of Nonsphericity of Earth's Gravitational Potential on an Equatorial Synchronous Satellite," NASA Goddard Space Flight Center, Guidance and Control Section Report No. 43, 15 June 1962.

4. Williams, D. D., "Dynamics Analysis and Design of the Synchronous Communication Satellite," Hughes Aircraft Company TM-649, May 1960.

5. "Torques and Attitude Sensing in Spin-Stabilized Synchronous Satellites," American Astronautical Society, Goddard Memorial Symposium, Washington, D. C., 16-17 March 1962.

6. Lotta, J. G., "Syncom II Weight Status," Hughes Aircraft Company IDC 2243 11/183, 18 September 1962.

7. Williams, D. D., "Precision in Magnetic Field," private notes, 3 November 1960.

8. Bell Telephone Laboratories, "Telstar Symposium," Goddard Space Flight Center, Greenbelt, Maryland, 18 September 1962.

3. ADVANCED TECHNOLOGICAL DEVELOPMENT

DUAL-MODE TRANSPONDER

General progress is satisfactorily on schedule with no major problems encountered during this period.

Negotiations are under way for final specifications with Rantec on the dual-sideband filter (4170 mc and 4080 mc), the dual-filter hybrid (2112 mc) of the frequency translation transponder, and the bandpass filters (2085 mc and 2119 mc) of the multiple-access transponder. Preliminary breadboard design is under way on the 6390-mc dual-mixer, the 66-mc master oscillator, and the 144-mc beacon oscillator. Breadboard fabrication of the wide-band preamplifier and the IF amplifier has been completed, and procurement from Hycon Manufacturing Co., of the dual-filter hybrid (4170 mc) is in process. Drawings are complete for the dual mixer and stripline RF power splitter, and fabrication of models has begun.

Six 2112-mc isolators of the frequency translation transponder, three 2085-mc isolators, and three 2119.14-mc isolators of the multiple access transponder are being modified to meet Mark II frequency specifications. Final design on this prototype isolator configuration is being accomplished, particularly the determination of the garnet dimensions (Figure 3-1). A portion of the drawings for fabrication of these 12 isolators are completed.

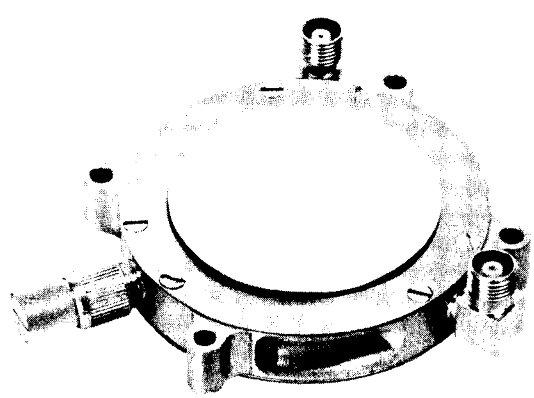

Figure 3-1. Isolator Redesigned for Mark II Transponders

Output Relay Prototype RF Power Switch

Breadboard design is under way to prove the feasibility of the ferrite "latch" type RF power switch, which uses a ferrite circulator with a permanent magnetic field that can be switched electronically. Preliminary experiments indicate that the breadboard design will be operational. Size and weight will be less than the ferrite isolator design (4 ounces, 2.5 inches outside diameter, 0.5 inch thick) of Syncom I.

The switchable permanent magnetic circuit design of this prototype was successful, due to its low driving power requirement (instantaneous application of 3 amperes required-to-switch). It appears that the electrical specification of 0.2 db RF loss can be met.

A second model power switch, refined to lighter weight and smaller size, is expected to be the final package configuration. The input and output connectors are Type TNC.

TRAVELING-WAVE TUBE

The initial tube design has been completed, drawings have been prepared, and fabrication begun. The first developmental tube will be available for test during the next report period with additional tubes to be available at a later date. Anticipated beam efficiency is 25 percent, with the helix voltage of 1050 volts. Gain is expected to be approximately 35 db. The gun design may necessitate further refinement, following evaluation of the first tube. Consideration will be given to making the tube slightly longer than the present configuration to obtain higher efficiency. Completion of assembly of the first developmental tube is scheduled for the first week of October; parameter measurements are scheduled to be completed during the second week of October.

A triangulated barrel, used successfully in other tube designs, is being used. Because the manufacturing processes for this barrel are easier to control, quality is better. The helix temperature will be lower than that in the Mark I tube, and resistance to vibration will be increased.

PHASED-ARRAY TRANSMITTING ANTENNA

The 8-kmc breadboard antenna and control circuitry, which has been in operation, is being modified into a breadboard at 4 kmc as new components are developed (Figure 3-2). In Figure 3-3 a to f show the beam patterns obtained from the 8.8-kmc breadboard phased array antenna with the beam rotating and the traces representing different aspect angles separated by 10 degrees; g is calibration data for the above, and h shows the sinusoidal inputs to the analog circuits and the complex waveforms applied to the ferrite phase shifters. Initially the antenna and phase shifters will be replaced with minor modifications in the power amplifiers that drive the phase shifters. Eventually all the early breadboard digital and analog circuits will be replaced.

The IBM 7090 digital computer program used to determine the optimum configuration of the array has been modified to determine tolerances in the control circuits.

Array Development

Work is progressing on a parallel basis on both horizontally and vertically polarized elements. The breadboard elements are being fabricated with TM type connectors that join mating connectors on a base plate; in this way the individual elements are easily removed so that both type arrays can be studied to determine which is best.

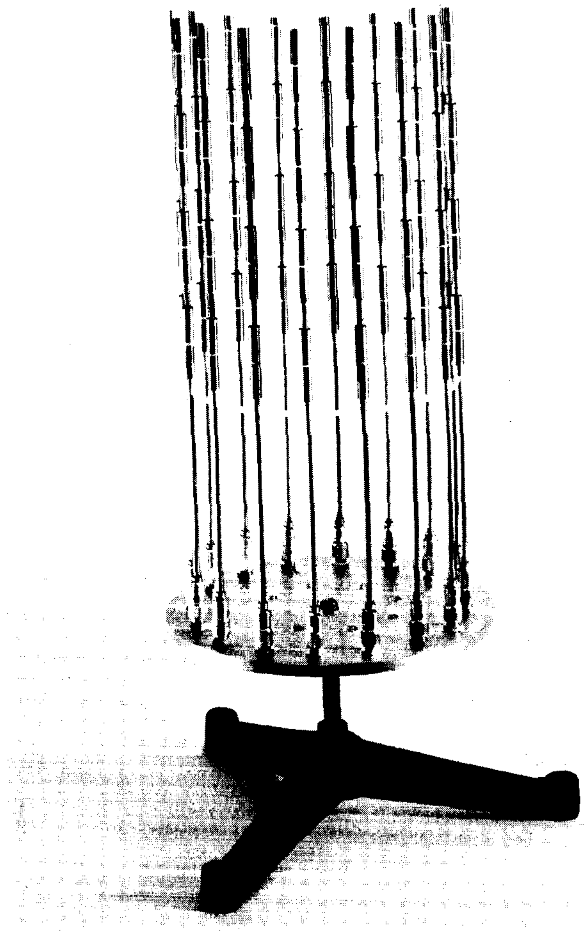

Figure 3-2. Initial Breadboard of 16-Element Vertically Polarized 4 kmc Antenna Array

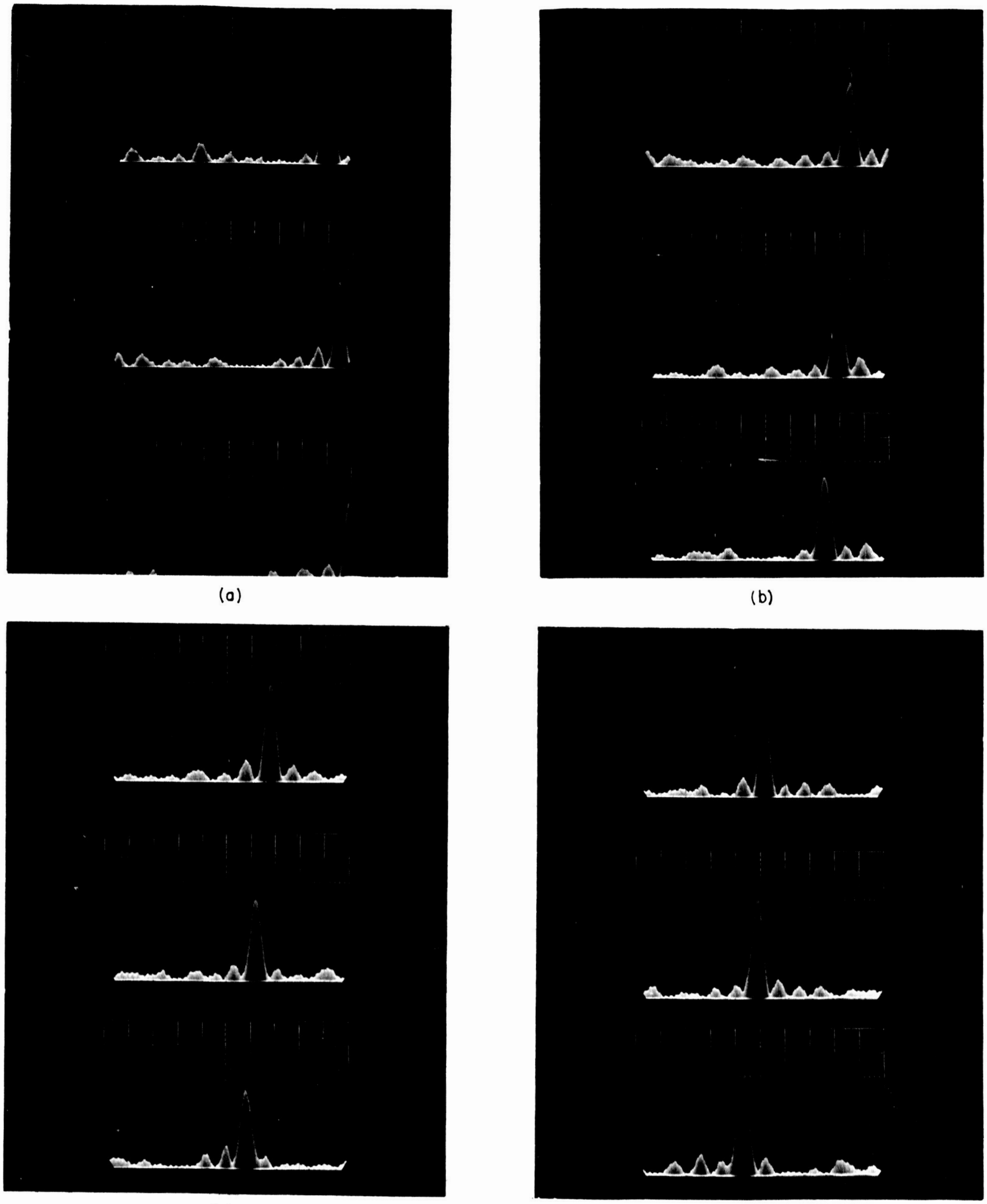

(a) (b) (c) (d)

Figure 3-3. Beam Patterns, Calibration Data, Sinusoidal Inputs and Complex Waveforms Obtained from 8.8 kmc Breadboard Phased Array Antenna

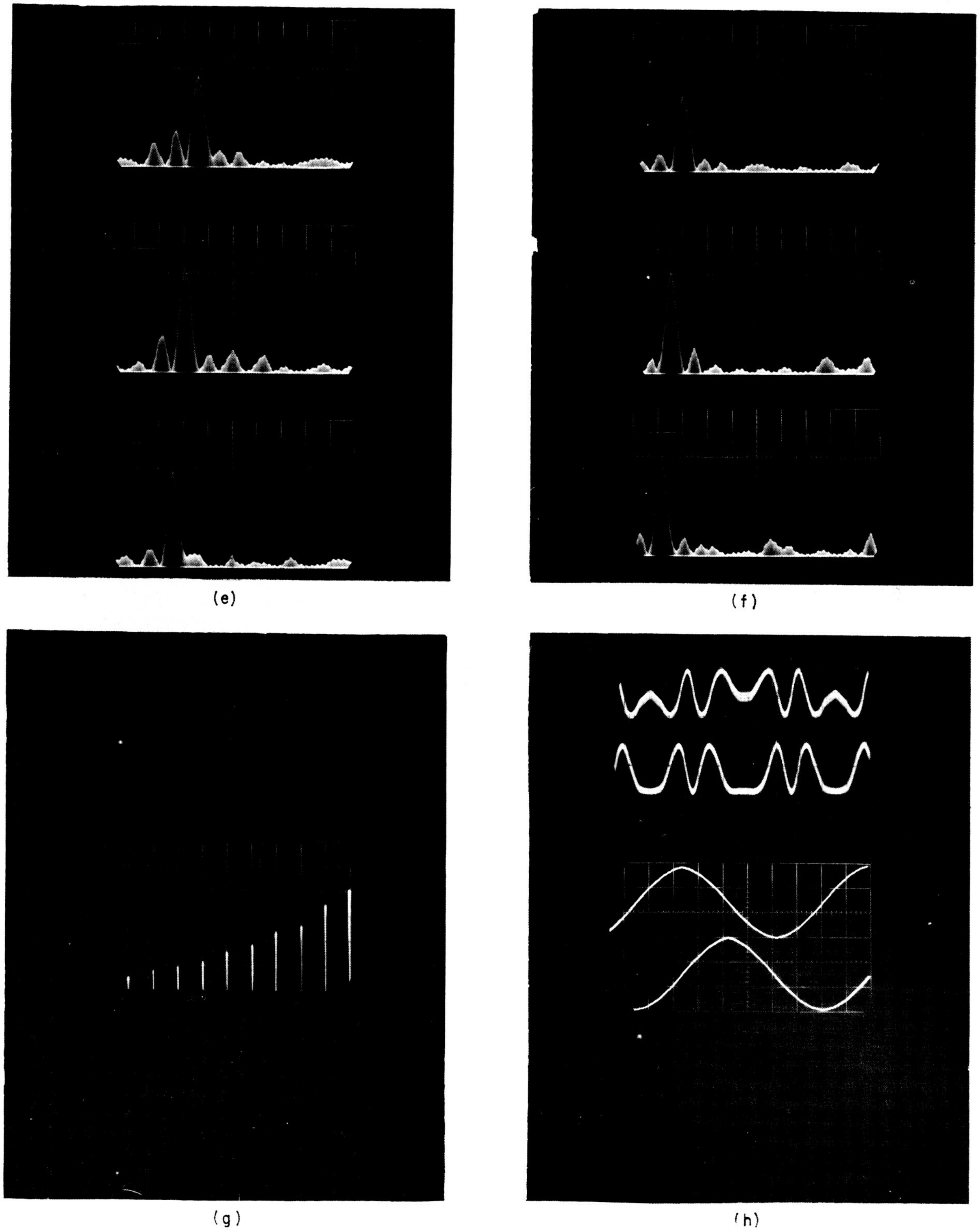

Figure 3-3. (Cont.) Beam Patterns, Calibration Data, Sinusoidal Inputs and Complex Waveforms Obtained from 8. 8 kmc Breadboard Phased Array Antenna

Vertical Polarization. The vertically polarized antenna elements have been scaled from the Syncom I transmitting antenna. Each element consists of a collinear array of four half-wave dipoles fed from gaps in the outer wall of a coaxial transmission line. A fiberglass sleeve for additional strength covers the element. The parts for all 16 elements have been fabricated and are being assembled. Each element will be matched and then assembled into the array for testing. Until the phase shifters are completed, static tests will be made by using coaxial feed lines cut to length. An exploded view of each element and a preliminary assembly are illustrated in Figure 3-4.

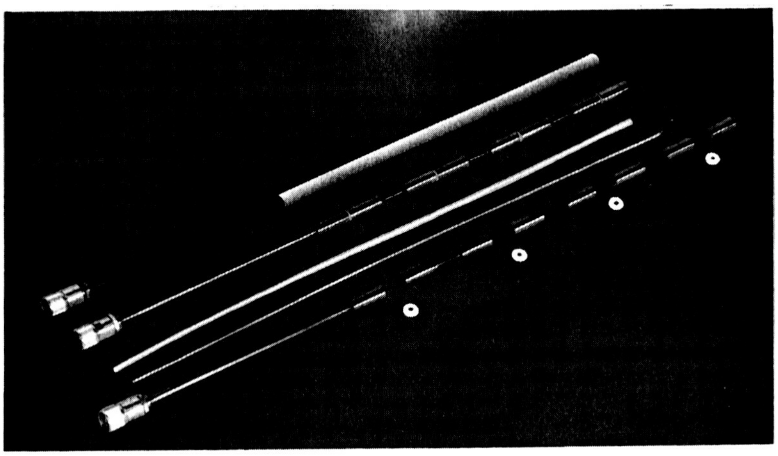

Figure 3-4. One Element of 16-Element Vertically Polarized 4 kmc Antenna Array

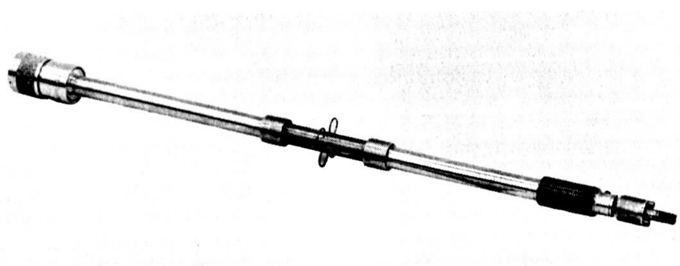

Figure 3-5. Cloverleaf Radiating Element

Horizontal Polarization. Design effort has been directed toward scaling a UHF cloverleaf antenna array to obtain the desired omnidirectional pattern with horizontal polarization. All tests to date used a single cloverleaf test section (Figure 3-5). The major problems encountered with this cloverleaf design were 1) obtaining the correct resonant frequency, 2) obtaining the desired coupling from the single cloverleaf, and 3) eliminating the stray currents flowing along the outside of the coaxial line, which give rise to end-fire beams of approximately the same amplitude as the desired broadside beam. Tentatively, the design problems were solved as follows:

1) The resonant frequency problem was solved first by decreasing the diameter of the four loops constituting the cloverleaf, which, however, resulted in lower coupling.

2) The coupling from the cloverleaf was increased to the desired amount by attaching a strip of metal to the outer edges of the loops of the cloverleaf (see Figure 3-6). The test data was taken with a mismatched connector on the coaxial test section, which contributed some error to the test results. This has been overcome by fabricating a special type N connector with a voltage standing wave ratio (VSWR) of 1.04:1, and this connector will be used in all future tests. The final cloverleaf configuration was asymmetrical, due to the many changes made in the development, and to omnidirectional pattern variations in amplitude by 6 db. A new symmetrical test section is being fabricated to be used in determining the final dimensions of the cloverleaf element, and also to insure omnidirectional radiation pattern when symmetry is maintained. When the final dimensions of the cloverleaf element have been determined, a five-element array will be fabricated with TM connectors.

3) The stray currents flowing on the outside of the coaxial line were eliminated by attaching suppressor wires to the loops of the cloverleaf at a point near where they emerge from the coaxial line, and shorting these suppressor wires to the outer surface of the coaxial line $\lambda/4$ down the line in each direction from the cloverleaf. An additional feature of the suppressor wire is its acting as a vernier control on the frequency, as the distance from the coaxial line to where the suppressor wire is connected is varied.

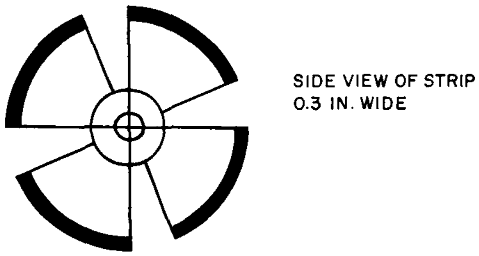

Figure 3-6. Outer Edges of UHF Cloverleaf Antenna Array

RF Circuits

The RF circuits include the power divider, the phase shifters and the feed lines to the antenna.

Ferrites. The type of ferrite to be used in the phase shifter has been tentatively chosen, based on tests of a number of samples. The ferrites have been ordered and delivery is scheduled during the next reporting period. Figures 3-7 and 3-8 illustrate the test fixtures and test setup used in evaluating the ferrites.

Input-Output Couplers. The couplers in and out of the phase shifters have been scaled from those used in the 8-kmc breadboard. Parts for the first coupler have been fabricated and are being assembled. If tests indicate satisfactory operation, the remainder of the couplers will be made.

Field Coils. The phase shifter field coils, in the form of motor stator windings, are on order from the manufacturer based on satisfactory tests of the initial sample.

Power Divider. The eight-way power divider, also scaled from the one in the 8-kmc breadboard, consists of seven hybrid rings made in strip-line. The ground planes are being fabricated and the artwork, prior to etching of the strip-line, is nearing completion.

Control Electronics. The final power amplifiers, which drive the field coils, have been redesigned to operate with the higher impedance windings used in the 4-kmc system. Other circuits are being redesigned to reduce the number of transistor amplifiers.

Digital Timing and Control Electronics

Block diagrams for the four subassemblies of the antenna phase control electronics have been completed and final logic equations released. Preliminary circuit releases have been made for 90 percent of the circuits, which represent 95 percent of the assembly components. A final circuit release of the tuning-fork oscillator was made and its specification has been prepared. Also, two forks have been ordered for the engineering model.

Critical parts of the subassemblies and all subassembly interfaces have been breadboarded and tested. Several dynamic problems were discovered and eliminated.

Extensive electrical tests were conducted on samples of small geometry, silicon, and planar transistors, from three different vendors. Data from these tests were used to write a general specification for this type of device. Two advantages were gained by this effort — enhanced electrical performance for the high usage transistor and decreased price.

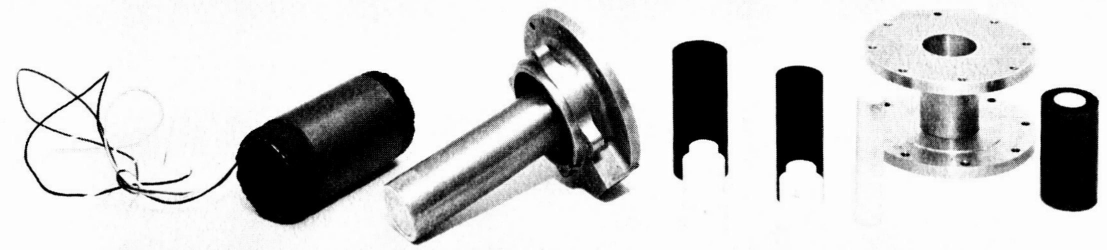

Figure 3-7. Test Fixtures Used for Evaluation of Ferrites for Phase Shifters

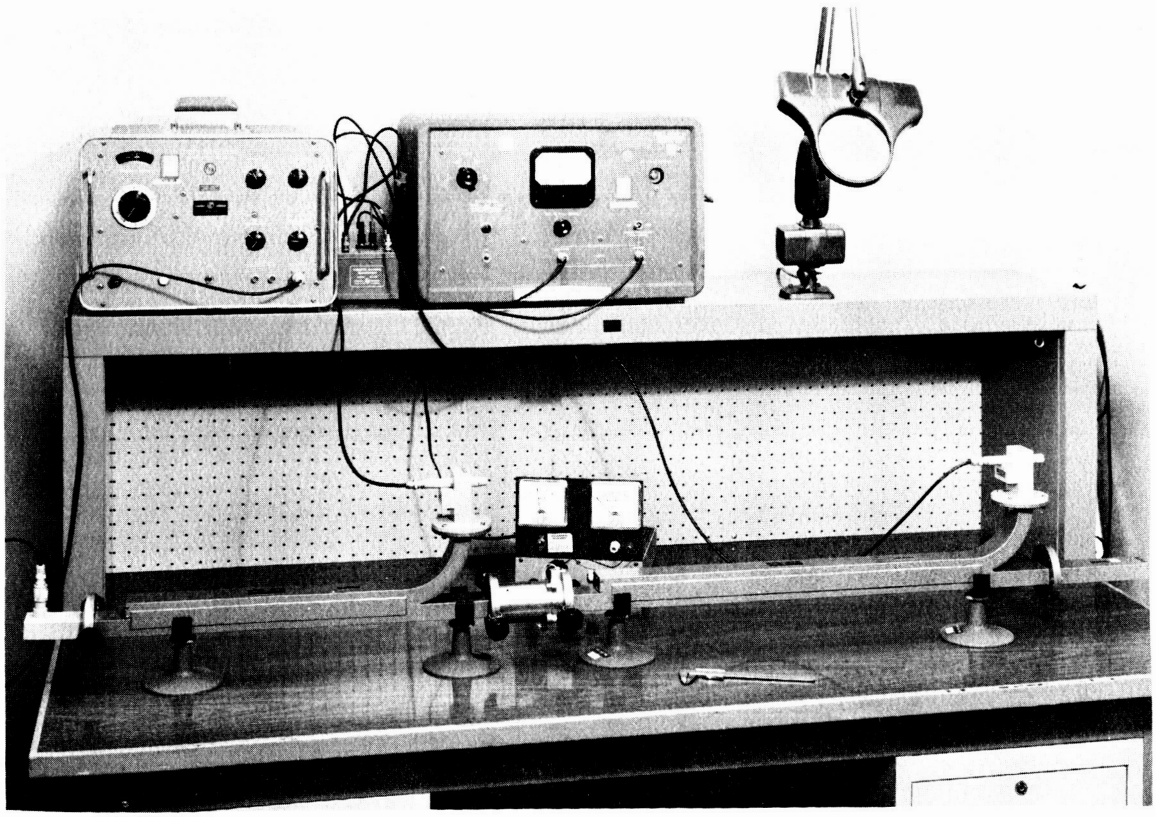

Figure 3-8. Complete Test Setup Used in Evaluating Phase Shifter Ferrites

The additional preliminary circuits will be released by 15 October, with final releases scheduled for 1 November. Figure 3-9 illustrates the overall block diagram.

COLLINEAR-ARRAY RECEIVING ANTENNA

The receiving antenna will be a skirted dipole array, similar to the transmitting antenna used in Mark I. The number of half-wavelength dipoles will be increased to four. By accurately exciting these dipoles in amplitude and/or phase, the gain will be optimized as the required beamwidth and bandwidth are obtained.

A linear array computer program, which includes the element pattern, is being used for pattern and gain calculations. The optimum gain (8. 6 db) for cophasal uniform distribution was found to occur with nearly 1-wavelength interelement spacing. The gain at this spacing is not too sensitive (with respect to the spacing), indicating the possibility of using an unloaded coaxial feed line (Figure 3-10). Many of the problems inherent in loaded lines could thus be avoided.

However, at one wavelength spacing, four dipoles give a beamwidth of only 13. 0 degrees, considerably less than the minimum allowed -17. 3 degrees. One approach to this problem has been to taper the distribution. With feeding coefficients of 0. 5, 1, 1, 0. 5, beamwidth and gain were 15. 1 degrees and 8. 2 db. Larger tapers are also being calculated. Also, due to the gain insensitivity described above, calculations are being made for 0. 9 λ spacing, with cophasal elements; this decrease in spacing will produce beam broadening.

Another solution might be possible in the use of nonuniform spacing of the elements to introduce controlled amounts of phase error, which would broaden the beam by the desired amount. The broadband impedance matching characteristics of such an array will be determined from existing computer programs. As an aid to these studies, a separate general computer program has been written for calculating the feeding coefficients as a function of the frequency or element spacing.

Structural Design

The initial selection of magnesium for the thrust tube is being reevaluated. Investigations are being made of an aluminum sand casting and a built-up thrust tube made of two machined rings with an aluminum sheetmetal tube (riveting machined stiffeners to the tube). Investigations were conducted initially on a magnesium forged billet, but it was not possible to forge in the required length.

The material has been determined for the forward structure, consisting of a tubular truss-work frame (Figure 3-11) attached to the forward bulkhead. The forward end of the triangular truss has a mounting bracket to attach the

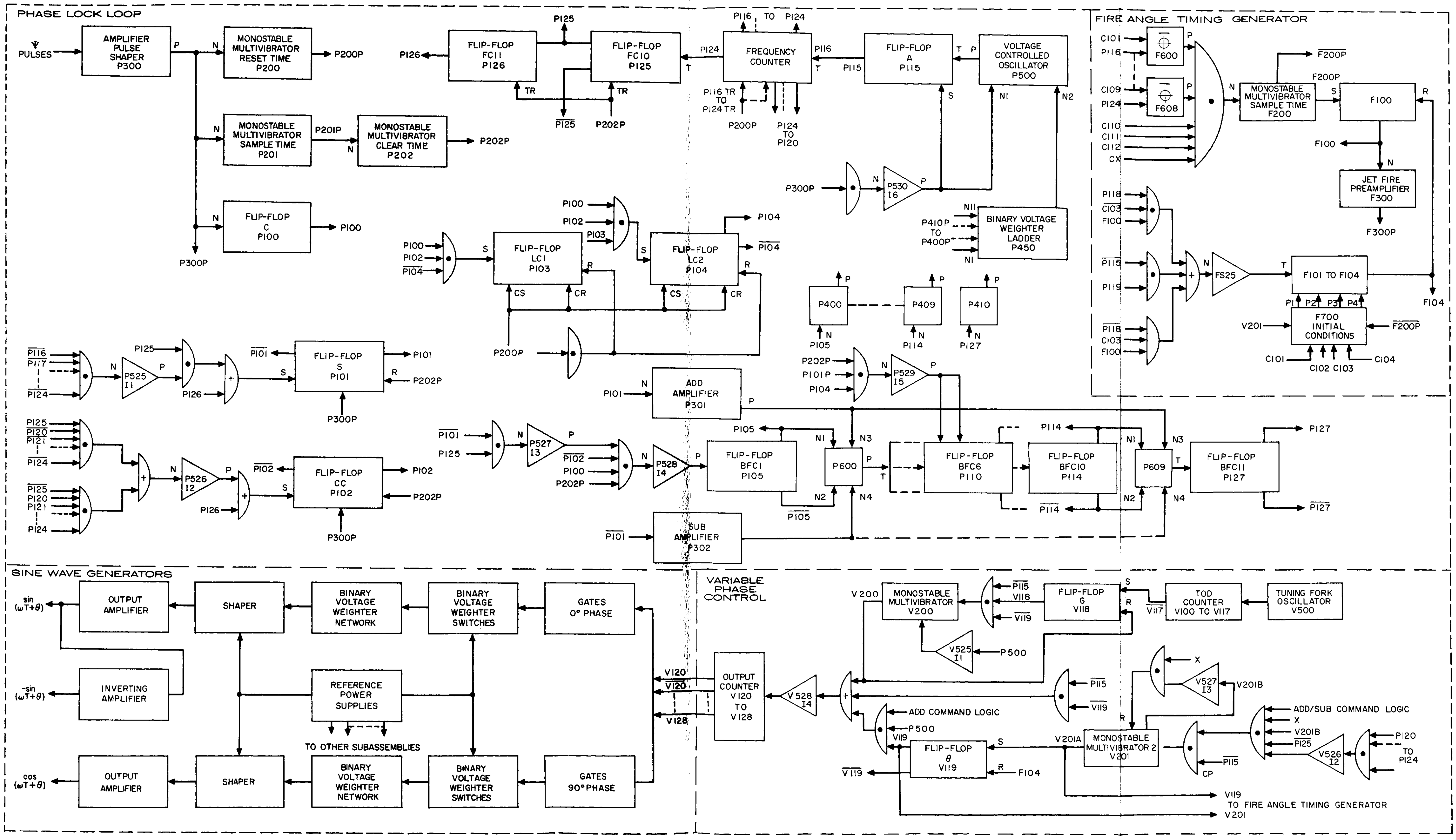

Figure 3-9. Phased Array Antenna Control Circuitry

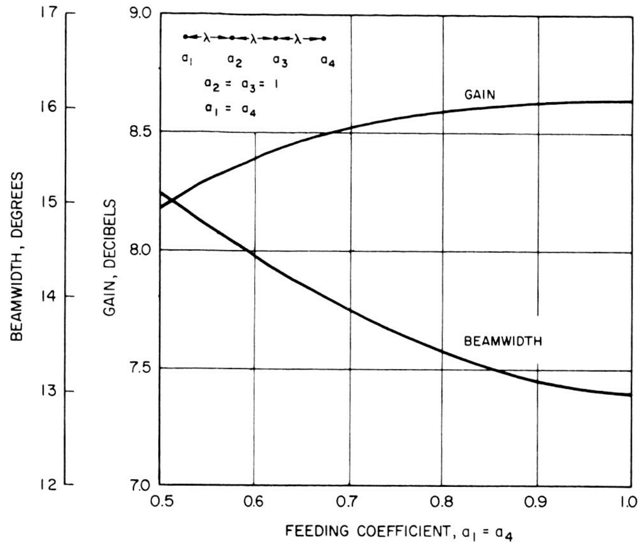

Figure 3-10. Gain and Beamwidth versus Amplitude of Outer Element Feeding Coefficients (a_1, a_4)

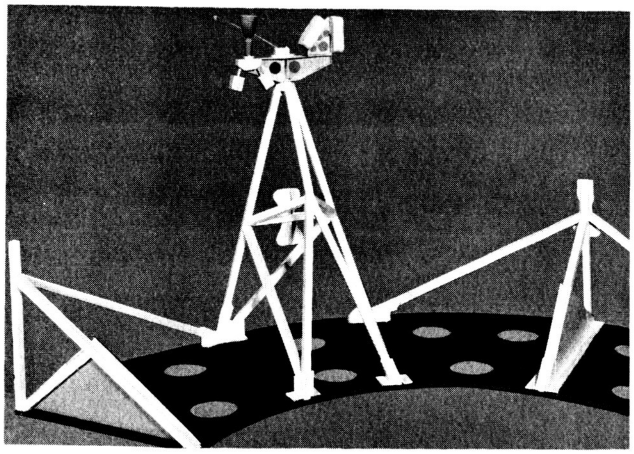

a) Outboard View

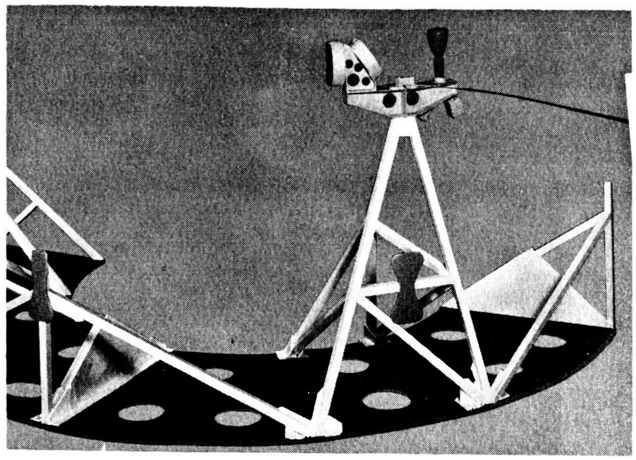

b) Inboard View

Figure 3-11. Tubular Truss Work Frame, Balsa Wood Mockup control system orientation jet, turnstile whip antennas, and a pair of V-beam sun sensors. In the center, the triangular truss-work has a solar cell panel mounting bracket.

Initial plans for magnesium 1/2 x 1/2 x 0.035 wall square tubing have been changed to aluminum 6061-T6, 0.500 outside diameter x 0.028 wall (round tubing). Changing to aluminum tubing, at a reduced weight, increased the strength and rigidity of the structure and decreased the deflection.

Drawings have been completed for the schematic of the bipropellant vernier control system (Figure 3-12) and its space envelope and mounting provisions (Figure 3-13). Detailed drawings are approximately 50 percent complete. The drawings of the forged ribs and cast thrust tube have been submitted for cost estimates.

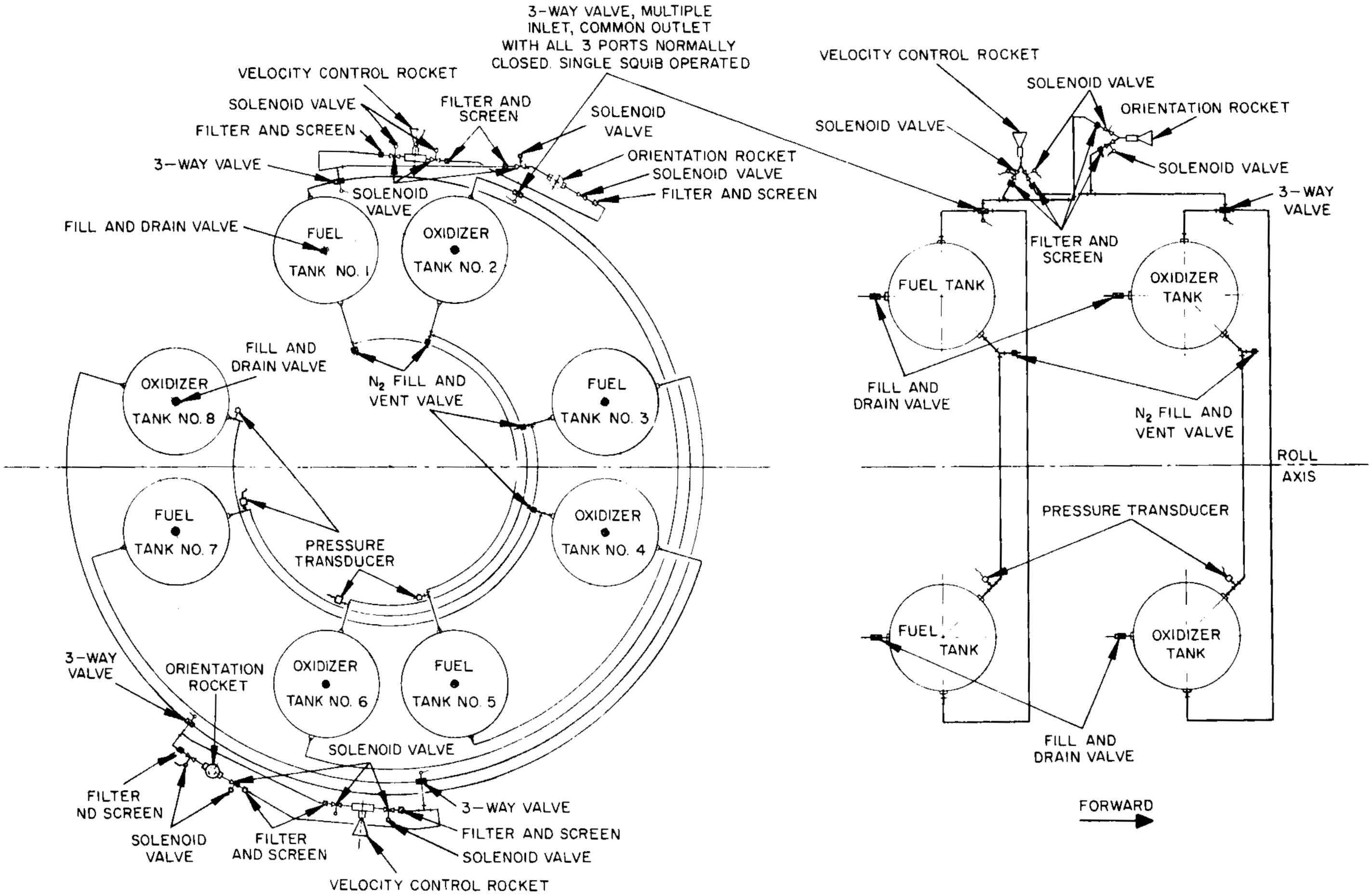

Figure 3-12. Schematic Diagram of Bipropellant Vernier Control System

Agena Interface

The thrust tube has been increased in length by 0.5 inch; it is now 18.937 inches long. This change increases the look angle of the antenna and affords more clearance area for release of the separation clamp. Lockheed has increased their clearance for the same reason.

The umbilical has been moved to the forward end of the spacecraft to give the phased-array antenna an unbroken horizon.

The interstage structure (furnished by Lockheed)(Figure 3-14) consists of a 45-degree (half-angle) cone, made with Fiberglas phenolic sheets riveted onto a framework consisting of eight metal hat-section stringers attached to rings at the top and bottom. The bottom ring attaches to the Agena D. The upper ring carries the spin table, which in turn attaches (by means of a three-bolt explosive clamp) to the spacecraft thrust tube.

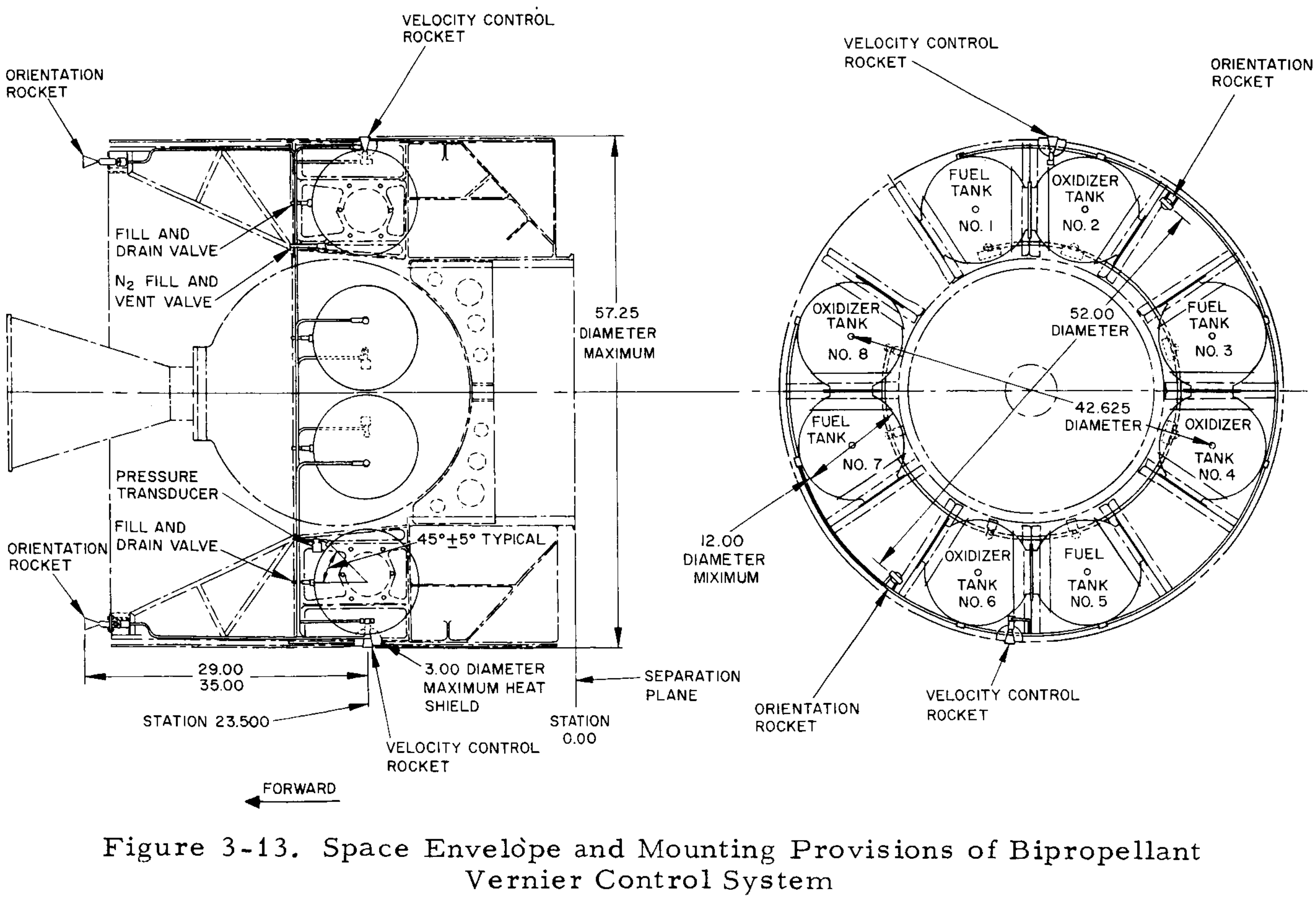

Figure 3-13. Space Envelope and Mounting Provisions of Bipropellant Vernier Control System

Structural Analyses

During the first portion of the developmental stage of the Mark II structure, emphasis has been placed in the following areas.

Lightweight Structure: Investigations have indicated that aluminum is more advantageous than magnesium from a stiffness viewpoint, plus other relevant considerations. Since the structure will be designed from a stiffness rather than a strength standpoint, effort is thus being made to optimize the structure, generally using aluminum. A rigid natural frequency requirement, such as that applied to Syncom I, will not be imposed on the Syncom II structure; nevertheless a goal of approximately 35 cps minimum lateral resonance frequency will be maintained.

Structural Design Criteria. Estimates have been made of the environment expected for the Syncom II satellite, utilizing information obtained from Lockheed reports. Additionally, investigations have been conducted into the structural dynamics of internal components such as the pressure tanks and apogee motor. Preliminary values of unit responses have been determined.

Coordination. Detailed liaison has been maintained between Hughes Structures personnel, Lockheed, and NASA.

Design Integration

Table 3-1 shows the latest weight estimate for the solid-propellant Mark II apogee motor configuration. Also included are the center of gravity and moment of inertia estimates for the spacecraft from separation through final orbit condition. The weight increase of the spacecraft in final orbit condition over that reported 15 August 1962 is, for the most part, directly attributable to the change in structural weight. This change requires added fuel weight to satisfy mission requirements with resulting spacecraft weight estimated at 1261 pounds at transfer orbit injection.

The initial concept of an all-magnesium structure has now changed to a design of one utilizing 60 percent magnesium by weight, and 40 percent aluminum. Thus, an additional weight penalty may be incurred with a continued change from magnesium to aluminum. The present ratio of structure-to-total-separated-spacecraft weight is 9 percent. The structural design is predicated on a spacecraft separated weight of 1530 pounds.

Present analysis indicates no problem areas in the ratio of roll-to-pitch moments of inertia.

Lengthening the thrust tube by 0.5 inch yielded a direct change from 23.0 inches to 23.5 inches in final orbit condition of the center of gravity along the axial plane from the interface.

Efforts during the next month will be spent in determining the liquid propellant system properties in roll and pitch, in addition to further refinements in design weight estimates. It is expected that a detailed weight report will be submitted in the next reporting period.

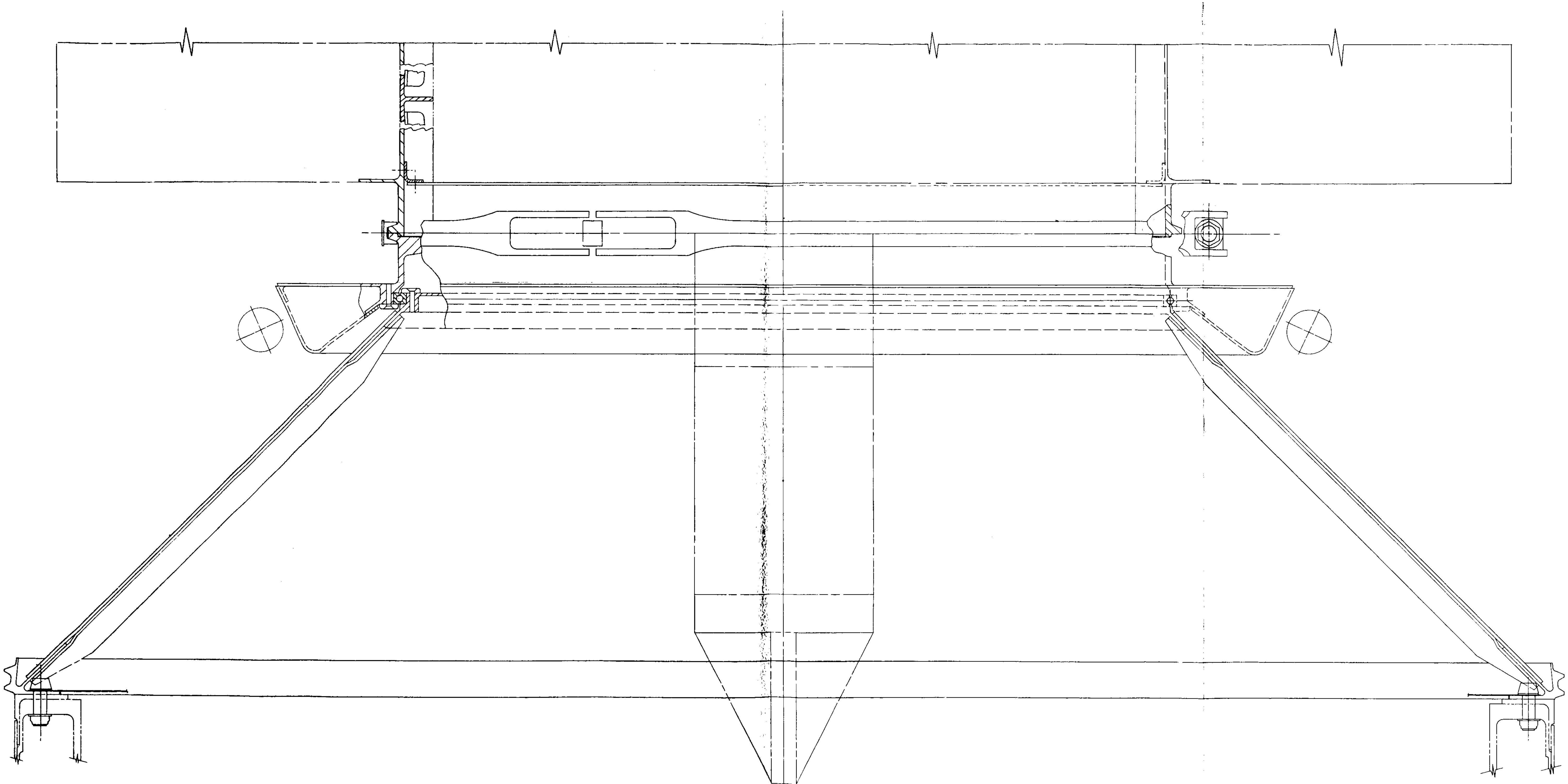

Figure 3-14. Interstage Structure

TABLE 3-1. SYNCOM II ESTIMATED WEIGHT STATUS

Subsystem	Weight, pounds
Electronics	130.0
Wiring harness	19.9
Power supply	99.1
Controls	38.6
Propulsion	75.1
Structure	115.5
Miscellaneous	16.1

	Weight, pounds	Z-Z	I_{ZZ}	I_{XX}	R/P
Final orbit condition	(494.3)	23.5	42.4	33.9	1.25
N_2 pressurization	3.2				
N_2H_3 - CH_3 fuel	55.6				
N_20_4 oxidizer	92.4				
Total at apogee burnout	(645.5)	23.5	59.5	42.2	1.41
Apogee motor propellant	615.3				
Total payload at separation	(1260.8)	24.5	70.8	54.0	1.31

THERMAL DESIGN

The primary effort in thermal control during the past month has been a close coordination with spacecraft design to ensure achievement of thermal control and to establish the requirements for testing thermal control surface coatings.

During the next reporting period the requirements for testing thermal control surface coatings will be finalized and documented. Additional investigation of semiactive temperature control devices will also be made.

HOT GAS REACTION JET CONTROL SUBSYSTEM

Primary effort has been directed towards defining functional requirements for the reaction jet system, preparation of the reaction jet system specification and RFP, preliminary design of the spin rate control mechanization, and review of the Syncom I sensor requirements for application to Syncom II.

Control System Design

During the next month the RFP for procurement of the hot gas system will be released, a configuration for the spin rate control device will be selected, and a detail design will commence. A heat transfer analysis of the spin rate control device will be initiated; studies of the Syncom I sun sensors and timers will continue; and an analysis of the stability of the orientation maneuver is under way. Problems that might arise with the selected bipropellant system are being investigated.

Bipropellant Rocket Reaction Jet Subsystem

Preliminary functional requirements have been established, and a list of studies and tests compiled for inclusion in the reaction jet specification.

Sun Sensors and Timers

The design of sun sensors and timers are undergoing modifications for Syncom I; it is expected that their designs will be applicable to the increased requirements of Syncom II. Availability of the spacecraft environmental requirements will allow further analysis of the adaptability of Syncom I components.

Spin-Rate Control Mechanism

Design efforts have been initiated on the control subsystem spin-rate control device hardware that will be fabricated and tested at Hughes. Due to the misalignments of the radial and axial jets, consistent with achievable mechanical tolerances, the thrust component tangential to the vehicle could cause the spin speed to vary by a factor of as much as three from the nominal 100 rpm. Therefore, spin speed correction is necessary. Because the axial jets are used

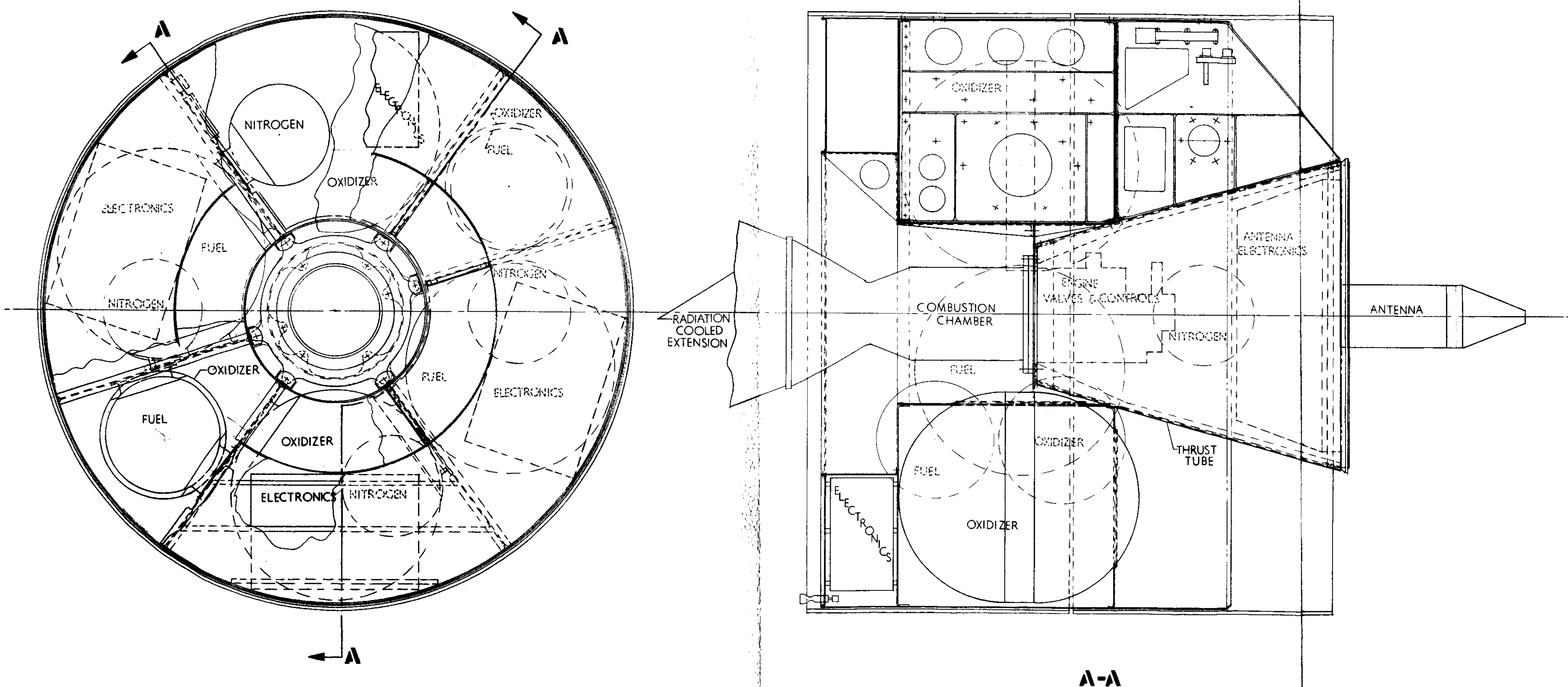

Figure 4-1. Combined Liquid Apogee Engine and Control System